Journal of Materials Chemistry C

Design and fabrication of flexible glucose sensing platform toward rapid battery-free detection of hyperglycaemia

Journal:	*Journal of Materials Chemistry C*
Manuscript ID	TC-ART-02-2021-000667.R1
Article Type:	Paper
Date Submitted by the Author:	29-Apr-2021
Complete List of Authors:	Fujita, Hajime; Tokyo Institute of Technology, School of Life Science and Technology Yamagishi, Kento; Singapore University of Technology and Design, Digital Manufacturing and Design (DManD) Centre Zhou, Wenshen; Singapore University of Technology and Design, Pillar of Engineering Product Development Tahara, Yu; Waseda University Huang, Shao Ying; Singapore University of Technology and Design, Pillar of Engineering Product Development Hashimoto, Michinao; Singapore University of Technology and Design, Pillar of Engineering Product Development Fujie, Toshinori; Tokyo Institute of Technology, School of Life Science and Technology

ARTICLE

Design and fabrication of flexible glucose sensing platform toward rapid battery-free detection of hyperglycaemia

Received 00th January 20xx,
Accepted 00th January 20xx

DOI: 10.1039/x0xx00000x

Hajime Fujita[a], Kento Yamagishi[b], Wenshen Zhou[c], Yu Tahara[d], Shao Ying Huang[c], Michinao Hashimoto[b, c], Toshinori Fujie[a,*]

The rapid detection of postprandial hyperglycaemia is imperative for the diagnosis of diabetes and the assessment of health risks for nondiabetics. Battery-free flexible glucose sensors are a promising tool for glucose sensing with a relatively low burden on biological tissues and living bodies because they are more lightweight and flexible than conventional battery-driven glucose sensors. However, existing battery-free glucose sensors are unsuitable for the practical detection of hyperglycaemia because of their long response time (> 1 h) and response fluctuation. In this research, we demonstrated a unique combination of materials and device design—phenylboronic acid (PBA) hydrogel integrated with an inkjet-printed interdigitated capacitor (IDC)—that enabled rapid response to the change in the glucose concentration. Specifically, the following three essential capabilities have been demonstrated: 1) quick response time (< 5 min) to mouse serum under hyperglycaemia in a battery-free setting, 2) conformability of soft PBA hydrogel suitable for the use on biological surfaces, and 3) controlled design of the signal transducer enabled by digital fabrication. We believe these capabilities serve as core technologies toward the development of tissue-interfaced battery-free glucose sensors with improved response time.

Introduction

Hyperglycaemia, caused by poorly regulated glucose metabolism and insulin resistance, is a major characteristic of diabetes. Excessive elevation of the postprandial glucose level is a general risk factor for obesity, hypertension, prediabetes, type 2 diabetes, and severe organ diseases[1,2]. In general, the postprandial glucose level reaches a peak at 30 to 60 min after food intake[3]. Thus, postprandial hyperglycaemia (PPHG) must be detected within 30 min. A flexible glucose sensor is the most efficient tool for detecting PPHG with minimal physical burden and preventing an increase in the risk of organ diseases, obesity, and diabetes[4].

Currently, battery-driven glucose sensors are widely used mainly among diabetic patients. Battery-driven glucose sensors instantly measure the glucose level and detect PPHG based on the rapid electrochemical transition on electrodes that mainly takes place between glucose and an enzyme such as flavin adenine dinucleotide-dependent glucose dehydrogenase (FAD-GDH)[5,6]. However, users have to replace such sensors as often as every two weeks due to a limited capacity of battery[7]. Also, the mechanical mismatch between a sensor electrode and the skin induced an inflammatory response in the surrounding tissue[8,9]. Battery-driven sensors have an advantage in the instant response, but the problems of the sensor-tissue integration are yet to be solved. To overcome this limitation, the development of battery-free flexible glucose sensors has been investigated. Battery-free devices designed to be lightweight and flexible can reduce a burden on biological tissues and living bodies.

Two types of battery-free glucose sensors have been demonstrated to date: (1) capacitive sensor based on phenylboronic acid (PBA) hydrogel[10–12] and (2) resistive sensor based on glucose oxidase (GOx)[13]. The battery-free sensors have a data transfer component coupled with a vector network analyser (VNA) in common, but they fabricated different types of signal transducers. Firstly, the existing battery-free capacitive sensor has a dual component of capacitive transducer and data transfer unit. The sensor consists of PBA hydrogel sandwiched between a set of coils coupled with VNA[12]. A set of the coils serves as both a capacitive detector of the PBA hydrogel and a data transfer component. When the volumetric change of PBA hydrogel takes place upon an elevated glucose level, the distance between the coils changes, resulting in the shift in resonant frequency on VNA. The capacitive sensors have a slow response (> 1 h) because of the slow volumetric change of the PBA hydrogel. On the other hand, the existing battery-free resistive sensor integrates a GOx-immobilized electrode with a data transfer component coupled with VNA[13]. In that study, the response time was as high as 2 h for a sensor attached to the eye of a rabbit that was fed to increase its glucose concentration

[a] School of Life Science and Technology, Tokyo Institute of Technology, 4259 Nagatsuta-cho, Midori Ward, Yokohama, Kanagawa 226-0026, Japan
E-mail: t_fujie@bio.titech.ac.jp
[b] Digital Manufacturing and Design (DManD) Centre, Singapore University of Technology and Design, Singapore 487372, Singapore
[c] Pillar of Engineering Product Development, Singapore University of Technology and Design, Singapore 487372, Singapore
[d] School of Advanced Science and Engineering, Waseda University, Shinjuku-ku, Tokyo 162-8480, Japan

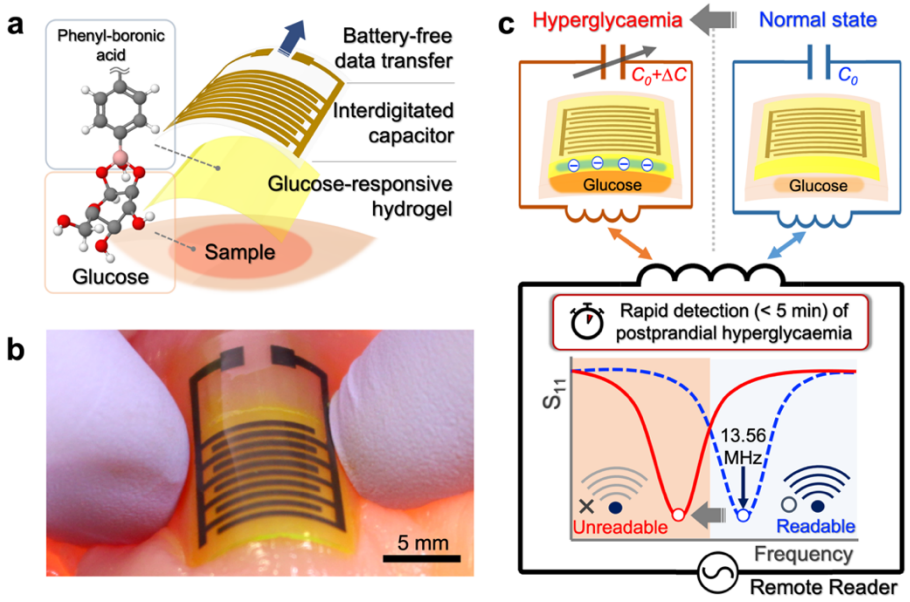

Fig. 1 Battery-free flexible glucose sensor for rapid detection of hyperglycaemia. (a) Layered structure consisting of glucose-responsive polymer hydrogel and an IDC. (b) Photograph of glucose sensor conforming to chicken muscle. The hydrogel layer was dyed yellow with fluorescein. (c) Scheme of battery-free detection of PPHG. The IDC detects the capacitive response to glucose in the PBA hydrogel and transmits it to an external reader in the form of a resonant frequency.

to a hyperglycaemic level. Overall, existing battery-free glucose sensors do not meet the requirements of the response time of 30 min for detecting PPHG[3].

To address the current limitation of the battery-free glucose sensors, we proposed and demonstrated the use of PBA hydrogel uniquely combined with digitally fabricated electrodes patterned on a flexible substrate. Specifically, we integrated PBA hydrogel with a flexible, inkjet-printed interdigitated capacitor (IDC) which can instantly detect a dielectric transition in PBA hydrogel. The signal transducer of PBA hydrogel and IDC is connected to a data transfer component coupled with VNA for the battery-free signal readout. In this study, we presented the following three capabilities that offer key advances in the development of battery-free flexible glucose sensors. Firstly, a quick response time (< 5 min) to mouse serum under hyperglycaemia was demonstrated by optimizing the thickness of PBA hydrogel (as thin as 200 µm). This response time is unprecedented and sufficient for detecting PPHG. Secondly, the conformability of PBA hydrogel was ensured for the tissue-interfaced sensing of glucose concentration. Lastly, controlled design and fabrication of signal transducer was achieved by inkjet printing and electromagnetic simulation, which enabled rapid prototyping and alteration of the device design. These capabilities serve as core technologies toward the development of tissue-interfaced battery-free glucose sensors with improved response time.

Results and discussion

Overview of this study

A proof-of-concept design of the proposed battery-free flexible glucose sensor (total thickness: 300 µm) is illustrated (Fig. 1a). The IDC served as a planar component that quickly detected the dielectric transition in PBA hydrogel. The controlled design of the signal transducer by inkjet printing and electromagnetic simulation contributed to the rapid detection of PPHG (< 5 min). In addition, the low flexural rigidity of the tissue-interfaced PBA hydrogel and the lightweight properties without battery on device ensured the conformability to biological tissues and living bodies (Fig. 1b and Fig. S1a,b in ESI). The scheme of the proposed battery-free detection of hyperglycaemia is illustrated (Fig. 1c and Fig. S2 in ESI). To demonstrate the capability of the battery-free sensor for tissue-interfaced applications, we examined its response to a hyperglycaemic level of glucose.

Design of battery-free flexible glucose sensor

We fabricated a thin-layer IDC on a flexible polyethylene terephthalate (PET) substrate using inkjet printing with Au nanoparticle ink (Fig. 2a). We selected an overhead projector film, namely surface-treated PET film (thickness: 100 µm), as the printing substrate because of its ink absorption characteristics and lower mechanical hysteresis than that of elastomer-based substrates[14–16]. We placed the IDC at the bottom of a silicone rubber spacer, on which PBA hydrogel was crosslinked (Fig. 2b). We added *N*-isopropylacrylamide (NIPAAm), which contains hydrophilic amide bonds and hydrophobic isopropyl groups, to the PBA hydrogel. The amphiphilicity of NIPAAm ensured a reversible phase transition of the hydrogel driven by the counterion osmotic pressure derived from negatively charged

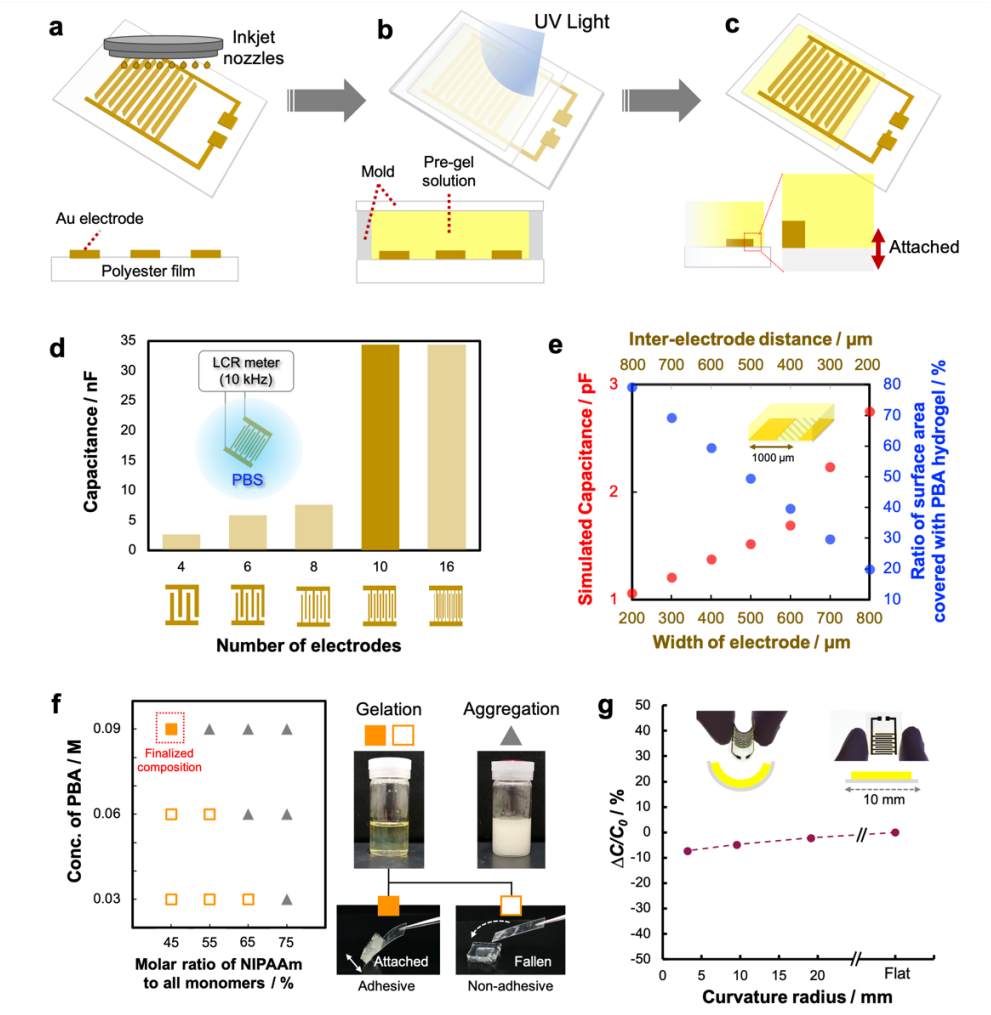

Fig. 2 Design of flexible glucose sensor consisting of an IDC and PBA hydrogel. (a) Fabrication of an IDC conducted by inkjet printing Au nanoparticle ink on PET film. (b) Layering of glucose-responsive hydrogel by photo-crosslinking. (c) Formation of layered structure. (d) Relationship between the number of inkjet-printed electrodes and actual measured capacitance. The parallel capacitance was measured in D-PBS(-) at 10 kHz. (e) Relationship between width of electrode and simulated capacitance of IDC surrounded by air (first y-axis), and ratio of surface area covered with PBA hydrogel (second y-axis) which is related to the stability of attachment between PET substrate and the hydrogel. (f) Relationship between the ratio of NIPAAm to all monomers and concentration of PBA; this relationship affected the adhesion between the PBA hydrogel and PET film (closed square: composition with successful gelation and sufficient adhesion as 5-mm-thick PBA hydrogel remained attached to PET film, open square: composition with successful gelation but poor adhesion as 5-mm-thick PBA hydrogel fell down from PET film, closed triangle: composition with unsuccessful gelation due to excessive phase separation and poor adhesion). (g) Relationship between curvature radius and change in capacitance and image and illustration of curved glucose sensor (left) and flat glucose sensor (right).

PBA when the glucose level became elevated[17,18]. After being crosslinked, the PBA hydrogel was attached to the IDC (Fig. 2c). The interconnection between the PBA hydrogel and the IDC was physically secured due to the hydrophilicity of the PBA hydrogel and the overhead projector film[19,20]. This layered structure served as the sensing element for battery-free glucose sensing. We optimized the design of IDC in terms of (1) the total number of electrodes, (2) the height of electrodes, and (3) the gap between the electrodes. The following equation was used to calculate capacitance *C*:

$$C = \varepsilon_0 \varepsilon_r \frac{A}{d} \quad (1)$$

where ε_0, ε_r, A, and d are the dielectric constant in a vacuum, the relative dielectric constant of the dielectric between electrodes, the area of facing electrodes, and the inter-electrode distance, respectively. We selected 10 electrodes based on the comparative analysis of capacitance with different number of electrodes in a fixed area (10 mm × 10 mm) (Fig. 2d). We optimized the capacitance of the IDC based on simulations conducted with several combinations of electrode width and inter-electrode distance, where the sum of the width and distance was fixed at 1000 μm (Fig. 2e)[21]. According to equation (1), the capacitance of the IDC can be increased by minimizing the inter-electrode distance. The inter-electrode area determines the mechanical stability of the interconnection between the PET substrate and PBA hydrogel. Given these

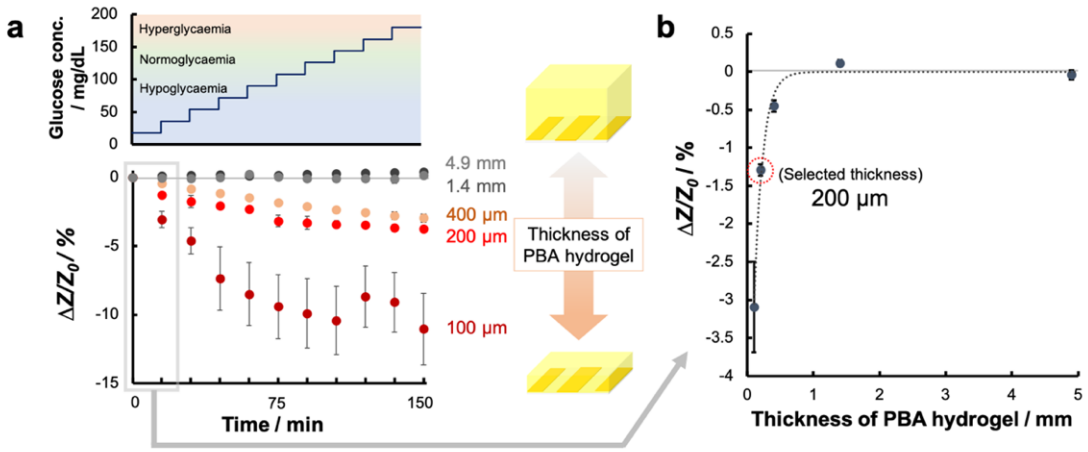

Fig. 3 Characterization of chemical-to-electrical signal transduction in PBA hydrogel. (a) Shift in impedance upon an incrementally elevated glucose level. The interval of glucose addition was 18 mg/dL per 15 min. Data are represented as mean ± standard deviation (SD) (n = 3). (b) Relationship between PBA hydrogel thickness and change in impedance upon an elevated glucose level (18 mg/dL) in 15 min. Mean ± SD (n = 3).

considerations, we selected 600 μm for the width of the electrode and 400 μm for the interelectrode distance based on simulated capacitance and ratio of inter-electrode surface area covered with PBA hydrogel which is related to the stability of attachment between the PET substrate and the hydrogel. In the simulation, the IDC design resulted in the capacitance of 1.7 pF and a ratio of the inter-electrode area to the entire printable area of 40%. We set the height of the electrode to 1 μm to ensure both sufficient simulated capacitance and flexural rigidity (7.99×10^{-9} N m) that is equivalent to the adjacent PBA hydrogel (1.51×10^{-8} N m) (Table 1, Fig. S3 and S4 in ESI). The Young's modulus and flexural rigidity of PBA hydrogel (1.79×10^{4} Pa and 1.51×10^{-8} N m) facing biological surfaces were lower than those of epidermis (1.02×10^{8} Pa and 1.10×10^{-5} N m) and dermis (1.02×10^{7} Pa and 3.73×10^{-3} N m) (Table 1). This result suggests that our sensor is mechanically conformable to the skin.

Table 1 Young's modulus, thickness, Poisson's ratio, and flexural rigidity of skin-interfaced PBA hydrogel and epidermis. The data are partially reproduced from ref. 22–26 and Figure S4.

	Young's modulus / Pa[22]	Thickness / mm[23,24]	Poisson's ratio[25,26]	Flexural rigidity / N m
PBA hydrogel	1.79×10^{4}	0.2	0.46	1.51×10^{-8}
Epidermis	1.02×10^{8}	0.1	0.48	1.10×10^{-5}
Dermis	1.02×10^{7}	1.5	0.48	3.73×10^{-3}

We also characterized the concentration of PBA and the ratio of NIPAAm to all monomers (Fig. 2f and Fig. S5a,b in ESI). We prioritized maximizing the concentration of PBA to ensure both a capacitive response to glucose and a stable interconnection between the PET substrate and PBA hydrogel. We also set the appropriate ratio of NIPAAm to ensure a dielectric transition[17,18]. PBA hydrogel indicated a slight volumetric change (< 5%) when the temperature increased from 25˚C to 35˚C, which is around skin or body temperature (Fig. S6 in ESI). This result suggests that temperature change would not affect the volume phase transition of PBA hydrogel[17,27,28]. Biofluids show various ionic strengths from the low level (0 mM in most beverages) to the high level (< 150 mM in ISF or blood)[12,29]. The previously demonstrated battery-free capacitive sensor indicated that 250-μm-thick PBA hydrogel maintained the dielectric response when the ionic strength of PBS changed from 150 mM to 35 mM and the pH changed from 7.4 to 6.5 and 8[12,30,31]. When the flexible sensor was bent, the capacitance value in PBS changed by at most 10%, and mostly by far less than 10% (Fig. 2g). When the curvature radius is set to 19 mm, the shift in capacitance is about -2%, which would result in the shift in resonant frequency by about 1%. This result indicates that the deformation of the sensing element did not significantly affect the sensor responses in both *in-vitro* setting (about -3% in 5 min) and *ex-vivo* setting (about -40% in 4 min).

Characterization of chemical-to-electrical signal transduction

Next, we evaluated the optimal thickness of the PBA hydrogel for electrochemical transitions and the capacitive response of the sensing element. We assessed the relationship between the hydrogel thickness and the electrochemical response of the sensing element to a glucose concentration increase from 0 to 18 mg/dL at pH 7.4 (Fig. 3a). The threshold thickness for the response was between 400 μm and 1.4 mm (Fig. 3b). The electrochemical response increased with decreasing hydrogel thickness. The diffusion time of glucose into 100-μm-thick planar hydrogel was estimated to be around 10 s[32]. A reduction in thickness speeds up the dielectric transition in the hydrogel[17]. Thus, a faster dielectric transition of the planar hydrogel in our sensing element could be achieved by minimizing the thickness.

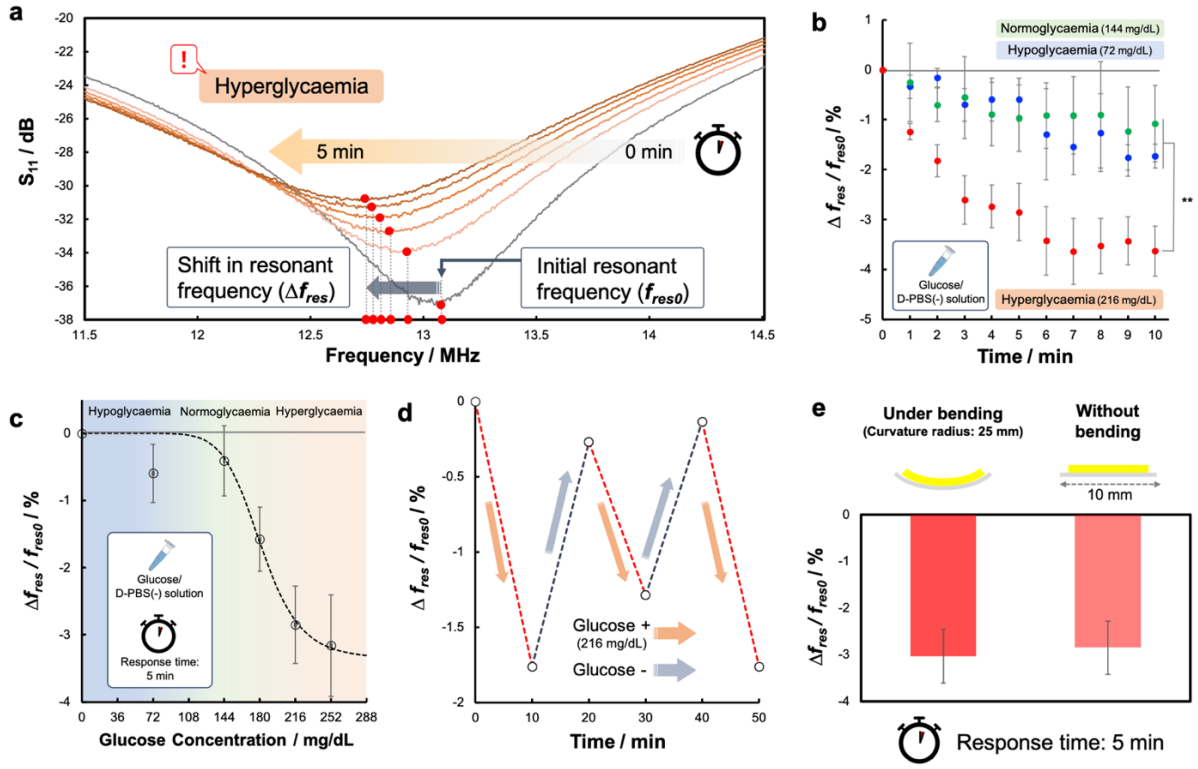

Fig. 4 *In-vitro* sensor response to changes in glucose concentration. (a) Response of sensor (shift in resonant frequency) to a hyperglycaemic level of glucose. Red spots on the graph indicate the peaks, and red spots on the x-axis correspond to the resonant frequencies. (b) Shift in resonant frequency under *in-vitro* setting. Mean ± SD (n = 3). The one-sided *P* values for the comparison of hyperglycaemic state (216 mg/dL) versus hypoglycaemic state (72 mg/dL) and hyperglycaemic state versus normoglycaemic state (144 mg/dL) were 0.0082 and 0.0089, respectively (95% confidence interval). ***P* < 0.01. (c) Relationship between glucose concentration and shift in resonant frequency measured 5 min after the addition of glucose. Mean ± SD (n = 3). Hill's equation was applied to the curve fitting. (d) Reversible shift of resonant frequency as a response to glucose concentration. (e) Comparison of shift in resonant frequency between bent sensing element (curvature radius: 25 mm) and flat sensing element. The shifts were calculated based on the sensor responses in 5 min under hyperglycaemic state (216 mg/dL). Mean ± SD (n = 3).

A sensor with 100-µm-thick PBA hydrogel indicated the highest response of impedance, but the deviation was by far larger than those with thicker PBA hydrogel. We selected 200 µm for the final thickness of the PBA hydrogel because this was the smallest thickness at which a high yield ratio was retained. To confirm the applicability of the proposed sensor to battery-free glucose sensing, we evaluated the PBA hydrogel's capacitive response to a hyperglycaemic level of glucose (216 mg/dL) at 13.56 MHz, a standard frequency in near-field communication (NFC). According to equation (1), the capacitance is linearly proportional to the dielectric constant. Under a hyperglycaemic state, the capacitance of the sensing capacitive response to glucose was sufficiently fast to detect PPHG, for which the glucose level reaches a peak at 30 to 60 min (Fig. S7)[3]. In general, the dielectric transitions in PBA hydrogel take place based on the following steps: (1) the diffusion of glucose molecules throughout the hydrogel, (2) a reversible reaction between glucose and negatively charged PBA derived from a hydroxide ion adduct, (3) an increased fraction of charged PBA in the hydrogel, (4) an increased counterion osmotic pressure between the hydrogel and external solution, and (5) the entry of external solution into the hydrogel (Fig. S8 in ESI)[17,27,28]. Previous battery-free capacitive sensor followed steps (1)-(5), resulting in the slow response (> 1 h)[12]. Our sensing element achieved the instant response (< 5 min) by following only steps (1)-(3).

In-vitro sensor response to changes in glucose concentration

We evaluated the response of the sensor (in terms of its resonant frequency) to three glycaemic levels, namely hypoglycaemia (72 mg/dL), normoglycaemia (144 mg/dL), and hyperglycaemia (216 mg/dL). We placed the sensing element at the bottom of a closed chamber and added PBS supplemented with glucose (final volume: 1 mL) into the chamber (Fig. S9a in ESI). We applied inductive coupling to the sensing element to transfer the capacitive response to the VNA in the form of a resonant frequency. The following equation was used to calculate the resonant frequency f_{res}:

$$f_{res} = \frac{1}{2\pi\sqrt{LC}} \quad (2)$$

where *L* and *C* are the inductance and capacitance, respectively. Before changing the glucose concentration, we applied

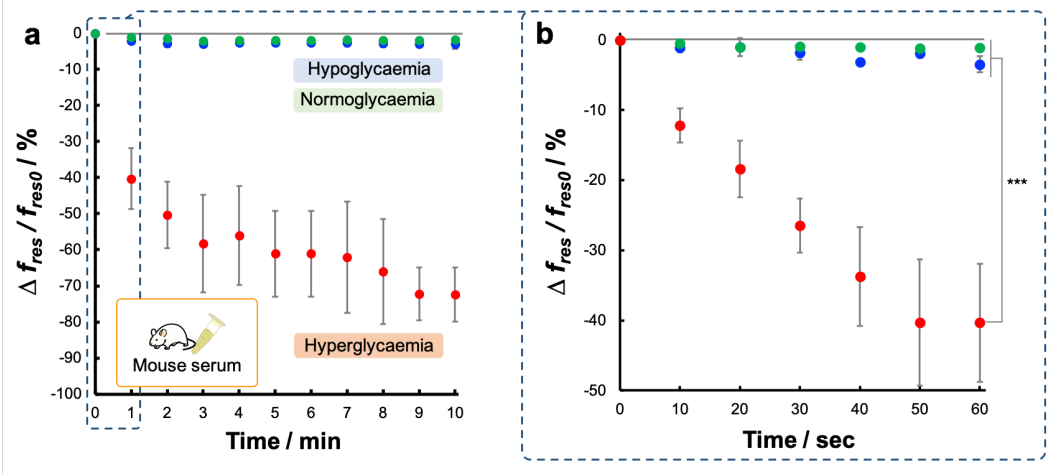

Fig. 5 *Ex-vivo* sensor response to changes in glucose concentration. (a) Shifts in resonant frequency under *ex-vivo* setting (a) 10 min and (b) 1 min after the addition of glucose. Mean ± SD (n = 3). The one-sided *P* values for the comparison of hyperglycaemic state versus hypoglycaemic state and hyperglycaemic state versus normoglycaemic state were both 0.0002 (95% confidence interval). ***$P < 0.001$.

impedance matching to the circuit and set the initial resonant frequency at around 13.56 MHz. We aimed to examine the capability of detecting a hyperglycaemic state and a non-hyperglycaemic state in the NFC range. Signals in this range can be detected by a commercially available remote reader. In this system, the resonant frequency shifts toward a lower frequency under a hyperglycaemic state. An instant alert of PPHG can be sent to the user after detecting the deviation of the resonant frequency from the NFC range or by quantifying the shift. The resonant frequency of the sensor shifted by about -3% (~ -400 kHz) in 5 min under a hyperglycaemic state (Fig. 4a and b). The *in-vitro* response within 5 min is shorter than those of previous battery-free glucose sensors based on PBA hydrogel (> 60 min)[11,12]. The inversion of the response between hypoglycaemia and normoglycaemia is attributed to the fluctuation of the peak, which can be observed in Fig. 4a. According to equation (2), the decrease in resonant frequency is attributed to the increase in the capacitance of the PBA hydrogel. The measurements under the hypoglycaemic and normoglycaemic states showed lower responses of only up to -2%. These results indicate that the sensor selectively detected a hyperglycaemic level of glucose. The relationship between glucose concentration and the shift in resonant frequency exhibits positive cooperativity that corresponds to a fitting curve obtained based on Hill's equation (Fig. 4c). Based on the sensing range of our sensor (0-252 mg/dL), we aimed to measure the glucose level in serum (88-124 mg/dL for healthy patients')[7]. We measured the shift in resonant frequency when PBS solution and the PBS solution supplemented with glucose (final concentration in the chamber: 216 mg/dL) were alternatively applied to the sensor via a syringe pump every 10 min (Fig. S9b in ESI). The flow rate was set to 2 mL/min so that the solution in the chamber could reach the target concentration within 3 min. We confirmed the sensor's reversible response to glucose by tracking the shift of the resonant frequency (Fig. 4d). The results from the *in-vitro* evaluation of the sensor response indicate that the glucose concentration can be tracked in the range of 0 to 216 mg/dL for at least two cycles (one cycle: 20 min). The responses in 5 min under bending (curvature radius: 25 mm) and without bending were equivalent (Fig. 4e). This result indicates that the deformation of the sensing element did not significantly affect the shift in resonant frequency under hyperglycaemic state.

Ex-vivo sensor response to changes in glucose concentration

Finally, we evaluated the *ex-vivo* sensor response to PPHG using a biological sample that contained foreign substances in addition to glucose (Fig. S9c in ESI). We placed the sensing element at the bottom of a closed chamber and added mouse serum (final volume: 100 µL) into the chamber (Fig. S9d in ESI). The resonant frequency decreased by ~60% 5 min after a hyperglycaemic level of glucose was reached (Fig. 5a). The resonant frequency shift under hypoglycaemic and normoglycaemic states was within a few percent. A large portion of the response to the hyperglycaemic state occurred within 1 min. The sensor could detect hyperglycaemic and non-hyperglycaemic levels of glucose in 10 s (Fig. 5b). Overall, the response of the sensor in the *ex-vivo* setting was larger than that in the *in-vitro* setting (PBS solution supplemented with glucose). The difference in the composition of dielectric compounds between *in-vitro* and *ex-vivo* specimens would bring about the enhanced sensor response under hyperglycaemic state. The serum contains foreign substances such as protein and the concentration of foreign substances in mouse serum might have differed at each glycaemic level. In order to normalize the effect of foreign substances on the dielectric transition in the hydrogel, we evaluated the response to fetal bovine serum (FBS) supplemented with normoglycaemic and hyperglycaemic levels of glucose (Fig. S10 in ESI). Specifically, we analysed the increase in the response from normoglycaemia to hyperglycaemia, and the increase in

the response to FBS was equivalent to that of *in-vitro* response to PBS. Therefore, our sensor can maintain the equivalent level of response to glucose in the presence of foreign substances. PBA reacts with not only glucose but also other compounds with *cis*-diol groups[35]. In serum, the concentration of compounds with *cis*-diol groups such as fructose is much lower than that of glucose[36]. Therefore, interference from compounds with *cis*-diol groups other than glucose is considered to be negligible.

Conclusions

In this research, we demonstrated important capabilities for the development of flexible battery-free glucose sensors. Our proof-of-concept prototype offered various properties superior to reported glucose sensors, including the response speed (< 5 min), the sensing range (0-252 mg/dL), and battery-free utility (Table 2).

Table 2 Sensor performance of reported battery-free and battery-driven glucose sensors. The data are partially reproduced from ref. 11, 12, 17 and 37.

Type	Example	Response time	Sensing range (mg/dL)
Battery-free sensor	This work	< 5 min	0-252
	Dautta *et al.* (2020)[12]	> 60 min	0-400
	Lei *et al.* (2006)[11]	> 60 min	0-360
Battery-driven sensor	Matsumoto *et al.* (2009)[17]	< 5 min	0-500
	Freestyle Libre (Abbott Laboratories)[37]	< 3 min	0-500

The sensor rapidly identified hyperglycaemia in serum by decreasing the thickness of the hydrogel embedded in it and detecting dielectric transition inside the hydrogel 5 min after the glucose level was elevated. The sensor consisted of a flexible polymer and conductive materials, allowing it to conform to biological tissues and living bodies. The sensor was small (< 10 mm × 10 mm) and thus applicable to the intermittent or continuous glucose monitoring of small animal models. The proposed design and fabrication process enhances response speed and improves a tissue-interfaced utility of battery-free glucose sensors.

We envisage the further development of the device as tissue-interfaced, battery-free glucose sensors. The sensing element of our sensor can be attached to the skin to detect the glucose level in blood[38] or ISF with microneedles for collecting specimen[39,40], or to detect the glucose level in sweat[6]. In the case of targeting the glucose level in sweat, the composition of the PBA hydrogel should be such that the sensing element can respond to the range of the target glucose level in sweat. The addition of a selectively permeable membrane as the top layer of the sensing element would prevent foreign substances such as proteins from interfering with the hydrogel's dielectric transition and the elution of polymers in the hydrogel[11]. To increase the biocompatibility, chitosan could be used in place of NIPAAm because of its responsivity based on the transitions in cationic amino groups and good long-term implantation outcomes[41,42]. Despite these challenges we are yet to address, we believe the demonstrated capabilities will offer a new paradigm for the design and prototyping of battery-free, flexible glucose sensors.

Experimental

Materials

Au nanoparticle ink (Au-J 0410B) was purchased from C-INK. Polyethylene terephthalate (PET) film (overhead projector film for monochrome inkjet printing) was purchased from AS ONE. *N*-isopropylacrylamide, acrylamide, 3-(acrylamide)-phenylboronic acid, and methylene bisacrylamide were purchased from Tokyo Chemical Industry. 2,2-Dimethoxy-2-phenylacetophenone and D-(+)-glucose was purchased from Sigma-Aldrich. Dimethylformamide and D-PBS(-) were purchased from FUJIFILM Wako Pure Chemical. The capacitor chip and inductor chip for impedance matching were purchased from Murata Manufacturing.

Fabrication of interdigitated capacitors

The performance of interdigitated capacitors (IDCs) with different designs was examined using simulation software based on finite element method (Femtet, Murata Software Co., Ltd.). The IDCs were fabricated with an inkjet printer (DMP-2831, FUJIFILM Dimatix). We selected inkjet printing for this patterning because of the ease of depositing ductile thin-layer electrodes and the customizability of electrode patterns[43–45]. The pattern of the IDCs (length: 10 mm, width: 600 µm, inter-electrode distance: 400 µm, number of layers: 3) was printed on an overhead projector film (dot spacing: 20 µm, plate temperature: 60 °C, number of nozzles: 1, number of layers: 3). We selected an overhead projector film, namely surface-treated PET film (thickness: 100 µm), as the printing substrate because of its ink absorption characteristics and lower mechanical hysteresis than that of elastomer-based substrates[14–16]. The printed IDCs were annealed at 100 °C for 3 h in a convection oven.

Preparation of glucose-responsive hydrogel on IDC surface

The monomers NIPAAm (0.6 M), AAm (0.6 M), 3-APBA (0.09 M), and BIS (0.03 M) and the photosensitizer 2,2-dimethoxy-2-phenylacetophenone (0.25 M) were dissolved in a mixed solvent consisting of 20 vol% dimethylformamide and 80 vol% deionized water. Silicone rubber spacer and coverslip were placed onto the electrodes, and the monomer solution was poured via a pipette into the space between the substrate and the coverslip. Photopolymerization was conducted by irradiating ultraviolet light (λ = 254 nm, 100 J/cm^2) through the coverslip. After the reaction, the coverslip was carefully removed, and the device was immersed in D-PBS(-) for 1 day to remove the dimethylformamide in the hydrogel.

Evaluation of flexural rigidity

The flexural rigidity (D) is defined by the following equation[43,46]:

$$D = \frac{Et^3}{12(1-\nu^2)} \quad (3)$$

where E is the Young's modulus, t is the thickness, and v is the Poisson's ratio.

Evaluation of the capacitance of IDC in PBS

We measured the capacitance for the different number of electrodes at 10 kHz using a handheld LCR meter (U1733C, Keysight Technologies). The sensing element was immersed in D-PBS(-) during the measurement. Also, we measured the change in capacitance for curvature radii of 19.1, 9.55, and 3.18 mm at 1 kHz using the handheld LCR meter. The sensing element was immersed in D-PBS(-) during the measurement.

Evaluation of the relationship between PBA hydrogel thickness and electrochemical response

To determine the relationship between PBA hydrogel thickness and electrochemical response, we prepared sensing elements with thicknesses of 100 µm, 200 µm, 400 µm, 1.4 mm, and 4.9 mm. An IDC with a unique design for this measurement (electrode length: 22 mm, electrode width: 1 mm, inter-electrode distance: 500 µm) was prepared. The sensing element was immersed in 30 mL of D-PBS(-) and connected to an LCR meter (IM3533, Hioki E.E.) via a four-port connection. We changed the glucose concentration from 0 to 18 mg/dL and measured the shift in impedance 15 min after the addition of glucose.

Evaluation of capacitive response to the hyperglycaemic level of glucose

The capacitance at 13.56 MHz was measured at room temperature by connecting the device to a vector network analyser (VNA) (E5063A, Keysight Technologies) via inductive coupling (number of sweeps: 1401, frequency range: 13.553 to 13.567 MHz, power: -5 dBm, intermediate frequency bandwidth: 10 kHz).

Battery-free detection of the *in-vitro* response to changes in glucose concentration

The device was connected to a VNA via inductive coupling. We added an LC circuit for impedance matching to set the resonant frequency at around 13.56 MHz. The shift in resonant frequency was measured at room temperature for various concentrations of glucose in D-PBS(-). The sensor was placed at the bottom of a cylindrical chamber filled with 500 µL of D-PBS(-). We mixed glucose into the D-PBS(-) and then added and pipetted 500 µL of the mixed solution to reach the final target concentration at the same time that the measurement was initiated. Glucose concentrations of 72, 144, and 216 mg/dL corresponded to the hypoglycaemic, normoglycaemic, and hyperglycaemic levels of blood glucose, respectively.

Evaluation of reversible response to changes in glucose concentration

The developed device was placed at the bottom of a cylindrical chamber and connected to a VNA via inductive coupling. Impedance matching was applied as described above. D-PBS(-) and a mixed solution of glucose and D-PBS(-) (glucose concentration: 216 mg/dL) were alternately injected into the chamber via a syringe pump (flow rate: 2 mL/min). The temperature of the entire system was maintained at 18 °C using a cool incubator.

Battery-free detection of *ex-vivo* response to changes in glucose concentration

The developed device was connected to a VNA via inductive coupling. The shift in resonant frequency was measured at room temperature. We initially filled the chamber with 500 µL of D-PBS(-) and replaced it with 100 µL of mouse serum. We started the data logging as soon as adding the sample and evaluated the shift in resonant frequency 1 min later. To prepare mouse serum under three glycaemic levels, 8-week-old mice were raised under identical conditions. Hypoglycaemic mice were prepared by removing the feed overnight. Normal mice were prepared by keeping the feed overnight. Hyperglycaemic mice were prepared by administering glucose via intraperitoneal injection at 2 g/kg body weight after feeding overnight. We took a blood sample from each mouse and measured the glucose concentration by blood glucose meter (Gluco Card PRIME, ARKRAY, Inc.) as soon as the blood collection. We centrifuged the blood samples and obtained serum at different glucose levels. The mean values of the hypoglycaemic, normoglycaemic, and hyperglycaemic levels were 73.8, 158.2, and 231.8 mg/dL. We prepared FBS with different glucose levels by simply mixing glucose to commercially available FBS. Following the same procedure as

mouse serum's, we evaluated the response to FBS (original glucose concentration: 110 mg/dL) and FBS supplemented with glucose (final glucose concentration: 224 mg/dL).

Author Contributions

Hajime Fujita: Writing - original draft, review and editing, Methodology, Conceptualization, Investigation, Validation, Visualization. **Kento Yamagishi**: Writing - review and editing, Conceptualization, Validation. **Wenshen Zhou**: Methodology, Validation. **Yu Tahara**: Writing - review and editing, Conceptualization, Investigation, Validation. **Shao Ying Huang**: Supervision, Validation. **Michinao Hashimoto**: Supervision, Writing - review and editing, Methodology, Conceptualization, Funding acquisition. **Toshinori Fujie**: Supervision, Writing - review and editing, Methodology, Conceptualization, Funding acquisition.

Conflicts of interest

There are no conflicts to declare.

Acknowledgements

This work was supported by JSPS KAKENHI (grant number 18H03539, 18H05469, 21H03815), MEXT Japan; Fusion Oriented REsearch for disruptive Science and Technology (FOREST), Japan Science and Technology Agency; the Tanaka Memorial Foundation; SUTD International Undergraduate Research Opportunities Programme; and JASSO Overseas Study Support Funding for H.F.'s stay at SUTD in 2019. T.F. is supported by the Leading Initiative for Excellent Young Researchers (LEADER) by MEXT, Japan. H.F. is supported by Tokyo Tech Academy for Super Smart Society (SSS) by MEXT, Japan. K.Y. and M.H. would like to thank Digital Manufacturing and Design (DManD) Centre at Singapore University of Technology and Design for the project support (RGDM1620403). H.F. and T.F. would like to thank A. Poon for discussions about electrical resonance, H. Sugime for discussions about the design of capacitor, C. L. Ken Lee for discussions about glucose-sensitive hydrogel, Y. Tetsu for assistance with data analysis, and T. Horii for assistance with electrical measurement.

Notes and references

1 D. Care and S. S. Suppl, *Diabetes Care*, 2020, **43**, S32–S36.
2 B. Gallwitz, *Diabetes Care*, 2009, **32**, 2, 0–3.
3 M. Takahashi, M. Ozaki, M.-I. Kang, H. Sasaki, M. Fukazawa, T. Iwakami, P. J. Lim, H.-K. Kim, S. Aoyama and S. Shibata, *Nutrients*, 2018, **10**, 1763.
4 D. Zeevi, T. Korem, N. Zmora, D. Israeli, D. Rothschild, A. Weinberger, O. Ben-Yacov, D. Lador, T. Avnit-Sagi, M. Lotan-Pompan, J. Suez, J. A. Mahdi, E. Matot, G. Malka, N. Kosower, M. Rein, G. Zilberman-Schapira, L. Dohnalová, M. Pevsner-Fischer, R. Bikovsky, Z. Halpern, E. Elinav and E. Segal, *Cell*, 2015, **163**, 1079–1094.
5 G. McGarraugh, *Diabetes Technol. Ther.*, 2009, **11**, 17-24.
6 A. Blum, *Clin. Diabetes*, 2018, **36**, 203–204.
7 D. Bruen, C. Delaney, L. Florea and D. Diamond, *Sensors*, 2017, **17**, 8, 1866.
8 S. P. Nichols, A. Koh, W. L. Storm, J. H. Shin and M. H. Schoenfisch, *Chem. Rev.*, 2013, **113**, 2528–2549.
9 B. Holt, A. Tripathi and J. Morgan, *J. Biomech.*, 2008, **41**, 2689–2695.
10 N. Y. Kim, K. K. Adhikari, R. Dhakal, Z. Chuluunbaatar, C. Wang and E. S. Kim, *Sci. Rep.*, 2015, **5**, 1–9.
11 M. Lei, A. Baldi, E. Nuxoll, R. A. Siegel and B. Ziaie, *Diabetes Technol. Ther.*, 2006, **8**, 112–122.
12 M. Dautta, M. Alshetaiwi, J. Escobar and P. Tseng, *Biosens. Bioelectron.*, 2020, **151**, 112004.
13 J. Kim, M. Kim, M.-S. Lee, K. Kim, S. Ji, Y.-T. Kim, J. Park, K. Na, K.-H. Bae, H. Kyun Kim, F. Bien, C. Young Lee and J.-U. Park, *Nat. Commun.*, 2017, **8**, 14997.
14 K. Takei, *J. Japan Inst. Electron. Packag.*, 2020, **23**, 347–352.
15 Y. Liu, M. Pharr and G. A. Salvatore, *ACS Nano*, 2017, **11**, 9614–9635.
16 C. Xu, Y. Yang and W. Gao, *Matter*, 2020, **2**, 1414–1445.
17 A. Matsumoto, N. Sato, T. Sakata, R. Yoshida, K. Kataoka and Y. Miyahara, *Adv. Mater.*, 2009, **21**, 4372–4378.
18 C. Zhang, M. D. Losego and P. V. Braun, *Chem. Mater.*, 2013, **25**, 3239–3250.
19 US Pat., US5413854A, 1995.
20 C. Wang, B. Lin, H. Zhu, F. Bi, S. Xiao, L. Wang, G. Gai and L. Zhao, *Molecules*, 2019, **24**, 1089.
21 S. Kanaparthi, S. Kayal and S. G. Singh, *Flex. Print. Electron.*, 2019, **4**, 015005.
22 F. M. Hendriks, D. Brokken, C. W. J. Oomens, D. L. Bader and F. P. T. Baaijens, *Med. Eng. Phys.*, 2006, **28**, 259–266.
23 P. Sejrsen, *Dan. Med. Bull.*, 1971, **18**, 3, 9-38.
24 S. Dahan, J. M. Lagarde, V. Turlier, L. Courrech and S. Mordon, *Dermatologic Surg.*, 2004, **30**, 872–880.
25 T. Takigawa, Y. Morino, K. Urayama and T. Masuda, *Polym. Gels Networks*, 1996, **4**, 1–5.
26 A. Delalleau, G. Josse, J. M. Lagarde, H. Zahouani and J. M. Bergheau, *J. Biomech.*, 2006, **39**, 1603–1610.
27 A. Matsumoto, T. Kurata, D. Shiino and K. Kataoka, *Macromolecules*, 2004, **37**, 1502–1510.
28 K. Kataoka, H. Miyazaki, M. Bunya, T. Okano and Y. Sakurai, *J. Am. Chem. Soc.*, 1998, **120**, 12694–12695.
29 R. H. Kretsinger, V. N. Uversky and E. A. Permyakov, *Encyclopedia of Metalloproteins*, Springer-Verlag New York, 2013.
30 Y. Marunaka, *World J Diabetes*, 2015, **6**, 125–135.

31 M. L. Halperin and K. S. Kamel, *Fluid, Electrolyte and Acid-Base Physiology*, Elsevier, 5th edn., 2017.
32 M. Ben-Moshe, V. L. Alexeev and S. A. Asher, *Anal. Chem.*, 2006, **78**, 5149–5157.
33 Q. J. Wan, P. Kubáň, J. Tanyanyiwa, A. Rainelli and P. C. Hauser, *Anal. Chim. Acta*, 2004, **525**, 11–16.
34 R. J. Gillespie and R. H. Cole, *Trans. Faraday Soc.*, 1956, **52**, 1325–1331.
35 J. P. Lor and J. O. Edwards, *J. Org. Chem.*, 1959, **24**, 769–774.
36 T. Kawasaki, H. Akanuma and T. Yamanouchi, *Diabetes Care*, 2002, **25**, 353–357.
37 FreeStyle Libre - Abbott Laboratories, https://www.freestyle.abbott/za/en/home.html, (accessed 29 April 2021).
38 C. G. Li, C. Y. Lee, K. Lee and H. Jung, *Biomed. Microdevices*, 2013, **15**, 17–25.
39 P. P. Samant and M. R. Prausnitz, *Proc. Natl. Acad. Sci. U. S. A.*, 2018, **115**, 4583–4588.
40 C. Kolluru, M. Williams, J. Chae and M. R. Prausnitz, *Adv. Healthc. Mater.*, 2019, **8**, 1801262.
41 N. Bhattarai, J. Gunn and M. Zhang, *Adv. Drug Deliv. Rev.*, 2010, **62**, 83–99.
42 F. L. Mi, Y. C. Tan, H. F. Liang and H. W. Sung, *Biomaterials*, 2002, **23**, 181–191.
43 N. Kokubo, M. Arake, K. Yamagishi, Y. Morimoto, S. Takeoka, H. Ohta and T. Fujie, *ACS Appl. Bio Mater.*, 2019, **2**, 20–26.
44 Y. Khan, F. J. Pavinatto, M. C. Lin, A. Liao, S. L. Swisher, K. Mann, V. Subramanian, M. M. Maharbiz and A. C. Arias, *Adv. Funct. Mater.*, 2016, **26**, 1004–1013.
45 L. Nayak, S. Mohanty, S. K. Nayak and A. Ramadoss, *J. Mater. Chem. C*, 2019, **7**, 8771–8795.
46 T. Yokota, P. Zalar, M. Kaltenbrunner, H. Jinno, N. Matsuhisa, H. Kitanosako, Y. Tachibana, W. Yukita, M. Koizumi and T. Someya, *Sci. Adv.*, 2016, **2**, e1501856.